Response to Referees for Wind Energy Science submission: Accurate loads and velocities on low solidity wind turbines using an improved Blade Element Momentum model by Yassine Ouakki and Abdelaziz Arbaoui

Dear Referees,

We would like to thank the reviewers for their comments and guidance to improve the quality of our manuscript. The manuscript is submitted for publication in the special issue "Wind Energy Science Conference 2019" in Wind Energy Science journal. Comments from Reviewer 1 and Reviewer 2 are addressed here. The main changes to the manuscript are listed below:

- We rewrote the abstract to highlight the contribution of the article. The paper concentrate on two second-order effects, that are important for low solidity rotors.
- We updated the introduction by including additional references, proposed by reviewer 1, on other second-order corrections. The relative importance of these second-order effects is discussed for the case of a low solidity rotor.
- The method section is also updated by further clarifying the derivation of the proposed improvements to the classical BEM method. The hypothesis of excluding the drag force when computing the induced velocities is no longer considered in the manuscript.
- The results and discussion section is also updated for the changes made in the method section.

Again, thank you for your time and suggestions to improve our manuscript. Please find below a detailed answer to your comments.

On behalf of the authors, yours sincerely,

Attached:

- Response to Referee 1
- Response to Referee 2
- Marked-up manuscript version.

Response to Referee 1

Dear Professor D.H Wood,
We would like to thank you for your detailed review of our paper. Your recommendations and comments improved the paper considerably. Please, see below a detailed response to your comments:

Comment 1: Blade element momentum (BEM) models have been used for many years for the aerodynamic analysis of wind turbines and propellers. Contrary to the statement on line 21, they were not introduced by Glauert (1935, reference in manuscript), who did however, develop them in a form that has been used for wind turbine analysis for nearly a century. For example, Lock et al. (1925, reference below) gives a detailed account of the pre-Goldstein (1929) and pre-Glauert version of BEM.
Reply 1: Indeed, Glauert (1935) was not the first to introduce the BEM theory. The 1D momentum theory was applied to an actuator dick by Rankine (1865). Then, the blade element theory was developed by Froude (1898) and made the first combination of both theories for propeller analysis. Later, Glauert (1935) finalized the BEM method by describing a full BEM model including wake swirl, turbulent wake state based on experimental data by Lock et al. (1925), and tip loss concept by Prandtl (1226).
Lock et al. (1925) work is not available online, so we couldn't give a detailed account of the pre-Goldstein and the pre-Glauert version of BEM.

Comment 2: Since the introduction of BEM, many second order corrections to it have been studied but these are not considered in the present manuscript. They include the effects of finite blade number, e.g. Clifton-Smith (2009), Wood et al. (2016), Schmitz & Maniaci (2017), Wimhurst & Willden (2017, 2018), the nonlinearity of the governing equations, Wood & Okulov (2017). Further, Limacher& Wood (2020) showed that the concerns of Goorjian (1972, reference in manuscript) over the role of the forces on the expanding streamtubes can be avoided easily. Therefore the claim in the manuscript to present a state of the art BEM analysis is not valid.
Reply 2: We have updated the introduction to include recent papers on second-order corrections of the BEM method. First, the effect of finite blade number, including the nonlinearity of governing equations, are further discussed in the introduction. Second, the concerns of Goorjian (1972) can be avoided using the impulse formulation Limacher& Wood (2020). However, the pressure term due to wake expansion is still present in the GMT formulation, which is applied to a low solidity rotor in the present work.
In the conclusion section, the "state of the art BEM model" is replaced by "an improved BEM model".

Comment 3: The manuscript concentrates on two aspects of BEM: the effect of wake expansion and an extension of the model of Bak et al. (2006) for rotational effects on the blade element forces. It is not demonstrated that these second order effects are more important than the others, but the reasonable agreement shown between the available measurements and the new model suggests that the contribution is worthwhile.
Reply 3: The proposed improvements to the classical BEM model were a new far wake expansion model and an extension of Bak stall delay model.
The relative importance of second-order effects can be analyzed based on the rotor geometry and tip speed ratio. First, the GMT is applied to a low solidity rotor, as a result the pressure drop due to wale rotation can be neglected. However, the wake expansion effect is retained because the 1D wake expansion model over-estimate the loading and also gives an unrealistic

expansion at a high tip speed ratio. The effect of a finite number of blades is accurately accounted for using classical Glauert correction at a high tip speed ratio, where the new far wake expansion is validated. However, at low tip speed ratio, Glauert tip loss still over-estimate the loadings and can be improved using Wood et al. (2016) model. To analyze and improve the 1D MT expansion model at a high tip speed ratio, Glauert tip loss model can be used with confidence. The BET is corrected to two second-order effects: stall delay and tip loss. Both effects are considered in this work.

Comment 4: The axial induction factors, a for the near-wake, and b for the far-wake, are assumed to be independent of radius, in for example, Equations (3) and (4). This is a major simplification which is not justified. Constant b in the far-wake gives a Joukowsky wake comprising a concentrated hub vortex of strength N where is the maximum bound circulation and N is the number of blades, and N helical vortices at the edge of the wake. Then the relation between pitch and far-wake velocity is easily determined from the Kawada-Hardin equations (Kawada, 1936; Hardin, 1982) as

$$\nu = 1 - \frac{N\Gamma}{2\pi h} \tag{1}$$

Where h is the vortex pitch, which contradicts Equation (12). For a Joukowsky wake, Wood (2007) rediscovered the result of McCutchen (1985) that the rotational velocity contribution to the energy equation is cancelled by the contribution of the radial pressure gradient, and so can be ignored, contrary to the statement of its importance made several times in the manuscript.

Reply 4: In the case of a Joukowski rotor, the rotational velocity contribution to the energy equation is canceled by the contribution of the radial pressure gradient (wood 2007 and McCutchen 1985). However, in Joukowski model, the maximum power coefficient is always is greater than the Betz limit. This problem was discussed by Sorensen and van Kuik (2011). It was suggested that the large increase in Cp at small tip-speed ratios is the lack of the lateral pressure on the control volume. Even though, lateral pressure is small, neglecting it will result an unrealistic power coefficient at low tip speed ratio. A similar problem arises in Glauert 1D expansion model (b=2a), where the expansion area increases toward infinity with increasing axial induction.

In this work, The axial induction factors (a and b) are not assumed to be independent of radius in the GMT (sorensen 2016). So, the wake is not a Joukowski one, since the only additional assumption to GMT is neglecting the pressure drop due to wake rotation (low solidity). However, Neglecting the lateral force (wake expansion) will result in unrealistic expansion at high axial induction. Even though this term is small, it induces an unrealistic expansion (1D expansion model) and also an over-estimation of loading for the full blade span. Glauert model assumes simply that the axial velocity at the rotor disk (U_n) is a mean value of upstream velocity (U_0) and far wake axial velocity (U_{nw}). This relationship is independent of operating conditions and rotor geometry. To overcome this inconsistency, the far wake expansion will be modeled using dimensional analysis, and it will be used to refine the Glauert model for the effect of wake expansion for low solidity rotors.

The relation between the pitch and far-wake velocity (Equation bellow) is first determined geometrically, then approximated for small expansion case by neglecting the velocity deficit. So, the pitch becomes dependent on known rotor parameters such as blades number, tip speed ratio.

$$h = 2\pi r tan(\Phi) \tag{2}$$

Where, Φ is the angle between the vortex sheet and the rotor plane.

Comment 5: It is also unlikely that the strength of the trailing vortices is set only by the lift on a blade element. When the angular momentum equation, (6) in the manuscript, is balanced against the blade element forces, the element drag is involved, and, therefore, the rotational induction factor a is partly determined by the drag. Since a is also the normalized circumferential velocity induced by the trailing helical vortices, the circulation of those vortices is also partly determined by the element drag.
Reply 5: Yes, the Joukowski theorem is only valid for inviscid flow, where drag force is zero. However, a generalized JK theorem includes the drag force (reference below). So the drag force will be included in the algorithm solution of BEM equations.

Li, Juan, YiZhe Xu, and ZiNiu Wu. "Kutta-Joukowski force expression for viscous flow." SCIENCE CHINA Physics, Mechanics & Astronomy 58.2 (2015): 1-5.

Comment 6: The manuscript is poorly written in places. For example, plane is often rendered as plan and there are many examples of poor expression which should be caught by a grammar checker.
Reply 6: Grammar was checked and gramatical correction where made.

Response to Referee 2

Dear Reviewer,

Thank you for your preliminary review of our paper. Your comments improved the paper considerably. Please see below a detailed response to your comments:

Comment 1: The parameter ξ is introduced wrongly just before Equation (11).
Reply 1: Corrected.

Comment 2: There is a bracket too much in the denominator of Equation (14)
Reply 2: Corrected.

Comment 3: In Equation (15) the term $\bar{h}$ in the square root in the denominator should be squared
Reply 3: Corrected.

Comment 4: Any explanation why the empirical parameters a_0 and b_0 are both chosen as 1 for this particular rotor (just after Equation (15)) is missing. Without any guidance on how to choose these parameters it is difficult to use the correction proposed in the paper.
Reply 4: In order to estimate the wake expansion ratio ξ, we applied the Buckingham π theorem to derive a physically meaningful equation (Equation 15) involving a certain number of dimensionless numbers (table 2). These dimensionless numbers can be further regrouped to form the apparent helical pitch $\bar{h}$.
By applying the π theorem, two constant parameters a_0 and b_0 need to be estimated. First, using the limiting case (λ converge to 0), the parameter a_0 is found to be equal to unity. The parameter b_0 has been estimated from experimental data of the NREL phase VI. Only data at one tip speed ratio is enough to estimate b_0. However, to cover a broader range of tip speed ratio, we used the data of the NREL phase VI at $U_0 = 5m/s, U_0 = 7m/s$, corresponding to a tip speed of 7.58 and 5.41 respectively. Comparing computed and measured distributions of normal and tangential forces, it was found that $b_0 \approx 1$ gives the best curve fit.

Comment 5: Equation (33) is not derived in the article and it is unclear where it comes from.
Reply 5: Bak et al. assumed that the chordwise flow is zero in the separated area, which is the same assumption made by Corten and Lindenburg to describe the centrifugal pumping mechanism due to rotation. Thus, the radial flow is assumed to be dominant compared to the chordwise flow. The centrifugal pumping mechanism is described as follows, the centrifugal force induces a radial flow, which in turn induce a chordwise Coriolis force that delays separation and amplifies the pressure in the separated area.
The normal force gradient was computed by integrating the pressure gradient over the full chord (Eq.29 in the manuscript), which contradicts the initial assumption that the rotational effect is present only in the separated area over the airfoil. Thus we proposed in this paper to estimate the normal force gradient by integrating the pressure gradient in the separated area only (Eq.33 in the manuscript). Additionally, assuming that the pressure gradient induced by the radial flow in the separated area mainly affects the normal force, thus the tangential force gradient can be neglected. The proposed improvement is consistent with the centrifugal pumping mechanism and the normal force gradient becomes dependent on the separation factor, which is a measure of the separated area on the airfoil.

Accurate loads and velocities on low solidity wind turbines using an improved Blade Element Momentum model

Yassine Ouakki[1] and Abdelaziz Arbaoui[1]

[1]INSCM team, LM2I, National School of Arts and Crafts (ENSAM), Moulay Ismail University, BP 4024 Meknes, Morocco

Correspondence: Yassine Ouakki (yassineouakki@gmail.com)

Abstract.

The accurate prediction of loadings and velocities on a wind turbine blades is essential for the design and optimization of wind turbines rotors. However, the classical BEM still suffer from an inaccurate prediction of induced velocities and loadings, even if the classical ~~correction~~ corrections like stall delay effect and tip loss correction are used. For low solidity rotors, the ~~loadings are generally over-predicted in the tip region, since the~~ far wake expansion is generally considered to be small, even at high tip speed ratio. In contrast, the 1D far wake expansion ~~is not accurately accounted for in the one-dimensional (1D) momentum theory. The 1D dimensional momentum theory supposes that~~ model gives an unrealistic expansion of the wake at a high tip speed ratio. This inconsistency is observed in Glauert model, where the far wake axial induction is ~~equal to~~ taken as twice the axial induction in the rotor plane~~, which results in an under-estimation of the axial induction factor in the tip region. Considering~~ . This unrealistic behavior of the 1D far wake expansion can be avoided by estimating the expansion ratio using dimensional analysis. Due to the complex nature of the flow around a rotating blade, the accurate estimation of 3D effects is still challenging, since most stall delay models still often tend to under-predict or over-predict the loadings near the root region. ~~As for the solution method for the classical BEM equation, the induced velocities are computed accounting for the drag force. However, according to the Kutta-Joukowski theorem, the induced velocities on a blade element are only created by lift force. Accounting for drag force when solving the BEM will result in an over-estimation of the axial induction factor, while the tangential induction factor is under-estimated.~~ To improve the accuracy of the BEM method, in this paper, the 1D momentum theory is corrected using a new far wake expansion model~~to take into account the radial flow effect~~. The blade element theory is corrected for three-dimensional effects through an improved stall delay model. ~~An improved solution method for the BEM equations respecting the Kutta-Joukowski theorem is proposed.~~ The improved BEM model is used to estimate the aerodynamic loads and velocities on the National Renewable Energy Laboratory Phase VI rotor blades. The results of this study show that the proposed BEM model gives an accurate prediction of the loads and velocities compared to the classical BEM model.

1 Introduction

Thanks to its simplicity and robustness, the blade element momentum (BEM) theory has been widely used in the wind industry for the design and optimization of wind turbine rotors (Tangler, 2002). ~~It was first introduced by Glauert (1935), as~~ The BEM theory is a combination of ~~the 1D~~ momentum theory (MT) and ~~the~~ blade element theory (BET). The 1D MT, ~~developed~~

~~by Glauert (1935)~~first proposed by Rankine (1865), is describing the process of energy extraction by the wind turbine rotor using the conservation laws of fluid mechanics. The BET, developed by Froude (1878) , is describing the local loadings and velocities ~~computation~~ computations on a blade element using airfoil theory. ~~Some assumptions in the BEM theory are corrected to make the prediction more realistic. The assumption of an infinite number of blades in the 1D MT is corrected using the Prandtl (1921) tip and hub loss model. The three-dimensional effects (3D stall delay) are also taken into account by correcting the 2D aerodynamic coefficients in the BET. However, The BEM model still suffers from its inaccurate prediction of induced velocities and the non-dimensional loading.~~

Later, Glauert (1935) finalized the BEM method by describing a full BEM method including wake swirl, turbulent wake state based on experimental data by Lock (1925) and tip loss concept by Prandtl (1921). Since then many engineering corrections were proposed to refine some assumptions in both theories. The 1D MT equations are ~~originally developed by Glauert (1935) by simplifying~~ derived from the general momentum theory (GMT) with additional assumptions. The first simplification was neglecting all nonlinear tangential velocity terms; as a result, the pressure drop due to wake rotation was neglected. The second simplification was using the GMT equation in differential form, which has been proven to be wrong by Goorjian (1972). Consequently, the axial induction in the far wake is taken as twice the induction at the rotor disc. Very recently, Limacher and Wood (2020) derived an impulse formulation having the advantage of avoiding the pressure term arising from the expansion of the streamtube, thus the concern of Goorjian (1972) can be avoided. However, the GMT formulation still accounts for the pressure term due to wake expansion.

Joukowski (1912) and Sharpe (2004) considered the effect of the pressure drop due to wake rotation, they found out that the rotor power coefficient increases at low tip speed ratio~~and can exceed the Betz-Joukowsky limit~~. Wood (2007) confirmed the finding of McCutchen (1985) that the rotational velocity contribution to the energy equation is canceled by the contribution of the radial pressure gradient. However, in Joukowski model, the maximum power coefficient is always exceeding the Betz limit and that it increases toward infinity at a low tip-speed ratio. This problem was discussed by Sørensen and van Kuik (2011) . It was suggested that the large increase in power coefficient, at small tip-speed ratios, is due to the lack of the lateral pressure on the control volume. Neglecting the lateral pressure, even if the lateral pressure is low, will result in an unrealistic power coefficient at a low top speed ratio. A similar problem arises in Glauert 1D expansion model, where the expansion area increases toward infinity with increasing tip-speed ratio. The influence of the pressure drop due to wake rotation is important for slow running rotors when the tip-speed-ratio is small (Vaz et al., 2011) . In contrast, For modern wind turbine rotors operating with ~~hight~~ high rotational speed and low torque (low solidity, typically 7% or less), the rotational kinetic energy in the wake will be small (Gupta and Leishman , 2005). As a result, the pressure drop due to wake rotation can be neglected. But, the use of an erroneous differential form of the GMT, will result in the cancelation of wake expansion by the pressure drop due to wake rotation. The power loss from wake rotation at a low tip speed ratio will be almost canceled by the increased mass flow through the rotor (De Vries (1979), Sharpe (2004), and Xiros and Xiros (2007)). However, at the level of spanwise loading, the wake expansion and pressure drop due to wake rotation do not cancel each other. In fact, The spanwise loading will be reduced at the tip region due to the presence of radial flow, and it will be augmented at the hub region due to the pressure drop due to wake rotation (Mast et al. (2004), Dossing et al. (2012), and Madsen et al. (2010)). Recently, Sun et al. (2016) proposed

an improved formulation of GMT accounting for both effects and found out that the axial induction factor in the far wake is always smaller than twice the axial induction at the rotor plane.

The classical BEM theory works well at low and moderate tip speed ratios, but it is not reliable at high tip speed ratios where the expansion of the wake is large (Sørensen et al. , 1998). ~~Whale et al. (2000) through~~ Through an experimental investigation Whale et al. (2000) found out that the wake expansion immediately behind the rotor becomes more pronounced towards high tip speed ratios. Carrión et al. (2015) performed a CFD analysis of the wake behind the Mexico rotor, They concluded that the higher the tip speed ratio, the more expansion of the wake. Recently, Micallef et al. (2013) performed a numerical and experimental investigation of the radial flow close to the rotor plane. They showed that the radial velocity reaches important magnitudes especially in the tip region and it is predominantly outboard, as a result, the wake expands. As for the root region, they found that there is almost no expansion of the wake. Herráez et al. (2014) has shown that the high axial induction will lead to an important wake expansion caused by a significant radial flow, especially in the tip region. Madsen et al. (2010) performed a comparison between the classical BEM and actuator disc. They found a close correlation between the AD and the classical BEM model for the integral value of the power coefficient. However, locally along the blade radius, they found that the classical BEM model overestimates the power coefficient and under-estimate the axial induction on the outboard part due to the wake expansion. Similarly, Johansen et al. (2004) found that a slightly lower induction in the tip region compared with the EllipSys3D computations. To correct the 1D MT, Madsen et al. (2010) proposed an empirical model to correct directly the induction for the expansion effect by fitting the AD simulations. Recently, Sun et al. (2016) proposed a generalized formulation of MT accounting for radial flow. However, in order to close the equation system, They used the semi-analytical AD equation of radial flow taken from the AD simulation by Madsen et al. (2010). Nevertheless, these BEM models are strongly coupled and require multiple iterative loops to be solved. As a result, they are computationally expensive compared to the classical BEM model, especially when used for the optimization of wind turbines rotors.

Considering the complexity of three-dimensional flow around a rotating blade, the non-dimensional 2D lift and drag, extracted from a wind tunnel for a given airfoil, fail to predict the aerodynamic loadings on a rotating blade at the inboard sections of the blades. In the last decades, extensive studies of this phenomenon were performed and several correction models were proposed (Spera (2009), Butterfield et al (1992), Lee and Wu (2013), Snel et al. (1993), and Breton et al. (2008)). These studies agree on the fact that for low wind speeds and angles of attack bellow the static stall angle, the flow remains attached to the blade and there is a minor difference between the lift and drag of a rotating blade and a non-rotating blade. ~~however~~However, when the 3D stall occurs at ~~hight~~ high angles of attack, the flow ~~began~~ begins to separate from the ~~blade surface~~ surface of the blade, and rotate with ~~the blade~~it. As a result, flow is subjected to rotational forces namely centrifugal and Coriolis forces. The centrifugal force induces an outboard radial flow, thus, the radial flow induces Coriolis forces that act as a favorable pressure gradient in the chord-wise direction. These forces lead to a delay in the separation process, resulting in an increase in the maximum lift coefficient at a higher angle of attack. This phenomenon is known as stall delay or rotational augmentation. However, based on the comparative study performed by Breton et al. (2008) on six existing stall delay models, they concluded that these models fail to predict the 3D behavior compared to NREL's phase VI experiment mainly because of their lack of generality~~since this phenomenon is not yet fully understood. However, compared to other stall delay models,~~

. Bak et al. (2006) model was found to have superior accuracy, compared to other stall delay models, thanks to the modeling approach that was based on estimating the pressure gradient instead of estimating the gradient of the force due to rotational effects. However, Bak et al. (2006) model is still over-estimating the loads. This original approach was adopted by Wang et al. (2013) to propose a new stall delay model by solving simplified Navier-Stocks equations for the pressure. Nevertheless, ~~these models~~stall delay models, that are based on estimating pressure gradient, are strongly empirical and showing a relatively good agreement with experimental data. However, Bak et al. (2006) model is not yet extensively validated, particularly, the force distributions along the blades (Breton et al. , 2008).

~~Moreover, The classical BEM model computes the induced velocities by solving iteratively the BEM equations accounting for the drag force. However, the induced velocities are produced by vortices (lift or circulation) according to vortex theory and particularly the Kutta-Joukowski theorem (De Vries , 1979). Thus, the induced velocities are only created by lift force. Lindenburg (2003)~~ The aerodynamic losses are present in both BET and MT. The MT assumes that the rotor has an infinite number of blades. In reality, the rotor has a finite number of blades and the blade has a finite span. Prandtl (1921) has shown that ~~in the case of a non-swept rotor blade , the relative induced velocity on the airfoil is a result of the circulation around it. Thus, it is perpendicular to the local relative flow. Wilson and Lissaman (1974) pointed out that the drag should be excluded from BEM equations because the drag-based velocity deficit is only a characteristic of the wake and it does not contribute to the induced velocity at the rotor disc~~the blade circulation tend to zero at the blade's tip. Later, Glauert (1935) proposed a simple approximation of Prandtl (1921) tip loss, which is commonly used in BEM codes. Glauert (1935) tip loss corrects the axial and tangential induction factors. Wilson and Lissaman (1974) and De Vries (1979) refined it by correcting the mass flux. De Vries (1979) correction was found to be the most suitable for blade optimization. However, the power coefficient improves about 1% compared to the BEM without tip loss (Clifton-Smith , 2009). Recently, ~~Shen et al. (2005) made a detailed analysis of BEM equations in the tip region. It was found that if we account for the drag force in the BEM equation, the relative velocity becomes zero at the tip , which is not physically true since the tip vortex is created at the blade~~ Wood et al. (2016) proposed three methods for direct calculation of tip ~~and then converted into the wake. Given these arguments, it is still arguably if the drag should be excluded from the BEM equations when computing the induced velocities (Burton et al. (2001) and Hansen (2015)). In either case, the drag force should be accounted for once the induced velocities are computed; since the drag force has an impact on the performance of a wind turbine rotor~~loss, using helical vortex theory, that improve the prediction for all tip speeds. Especially, at low tip speed where the classical Glauert correction is inaccurate. Later, Wood and Okulov (2017) analyzed the nonlinear terms in the thrust and torque coefficient due to finite number of blades . Nonlinear terms were found to be important in the tip region at a low tip speed ratio. Glauert (1935) tip loss model is adopted in this work because it is accurate at a high tip speed ratio, where the expansion effect is important. The blade element theory neglect the span-wise dimension effect by using 2D airfoil data to compute the loads near the tip, however, the loads should tend to zero at the tip allowing to pressure equalization Shen et al. (2005). The tip loss mechanism was studied by Wimshurst and Willden (2018), and it was attributed to the effect of the vorticity shedding from the outboard blade sections. Shen et al. (2005) proposed a modified tip loss of Glauert to take into account this kind of aerodynamic loss. Recently, Shen tip loss correction was re-calibrated in axial and tangential directions separately, using Mexico data (Wimshurst and Willden , 2017). Thus, improving the tangential loading

and power predictions. Schmitz and Maniaci (2017) adopted Shen et al. (2005) approach to correct the Glauert tip loss for the effect of tip roll-up vortex and wake expansion in the tip region.

This manuscript is organized as follows. In Section 2, the GMT is applied to low solidity wind turbine rotors, then a new far wake expansion model is proposed using dimensional analysis. In Section 3, the blade element model is described, then an improved stall delay model is proposed. In Section 4, ~~An improved BEM model respecting the Kutta-Joukowski theorem is given, the~~ The improved BEM equations are solved using the guaranteed convergence algorithm. In Section 5, A detailed validation of the proposed BEM model is performed based on the experimental results of the NREL Phase VI rotor (Hand et al , 2001). At last, the conclusion and further improvements of the BEM model will be given.

2 Improved momentum theory

2.1 General momentum theory applied to low solidity wind turbines

The general momentum theory (GMT) is based on a global description of the flow around the wind turbine rotor. The rotor is modeled as an actuator disc with an infinite number of blades. The flow is considered steady, incompressible, and axisymmetric. The GMT take into account the radial, axial and azimuthal ~~velocities~~variation of the flow. The axial and radial ~~velocity~~ velocities are continuous, while the azimuthal velocity has a discontinuity at the actuator disc. A rotation of the flow is present in the wake, and it is absent upstream of the rotor disc. The pressure drop at the rotor disc is due to the change in azimuthal velocity at the rotor disc (Sørensen , 2016). Assuming that the air masse contained in the rotor disc is separate from the rest of the air in the rotor plane, as a result, the air masse at the rotor disc can be contained in a circular boundary surface. It can be extended upstream and downstream of the rotor forming a long stream-tube of circular cross-sections. Since the air within the circular boundary of the stream-tube is assumed to be incompressible; the cross-sectional area of the stream-tube must expand to accommodate the drop in wind speed. Thus, the conservation laws of fluid mechanics can be applied globally along the stream tube or locally along an annular stream tube (see Fig. 1).

The annular element of the actuator disc is taken at a radial position r and the actuator disc rotating with a rotational speed noted Ω. The annular element at the far wake is taken at a radial position r_w and rotating with a rotational speed noted ω_w. Due to the discontinuity in the rotational motion of the flow at the rotor plane, The tangential velocity at the rotor disk is taken as the average of the upstream and downstream plane $V_t = -r\Omega a'$. Since there is no rotation of the flow in the upstream ~~plan~~plane, the tangential velocity is zero upstream of the rotor $V_{t+} = 0$, the tangential velocity straight after the rotor $V_{t-} = -2r\Omega a'$, and $V_{tw} = -r_w\omega_w$ in the far-wake. In contrast, the axial and radial velocities are continuous, thus the radial and axial velocities straight after and before the rotor are identical. The radial velocity in the far upstream and ~~downstream plans~~ far downstream planes is zero since there is no expansion of the far upstream and downstream wake. In the rotor plane, the radial velocity is

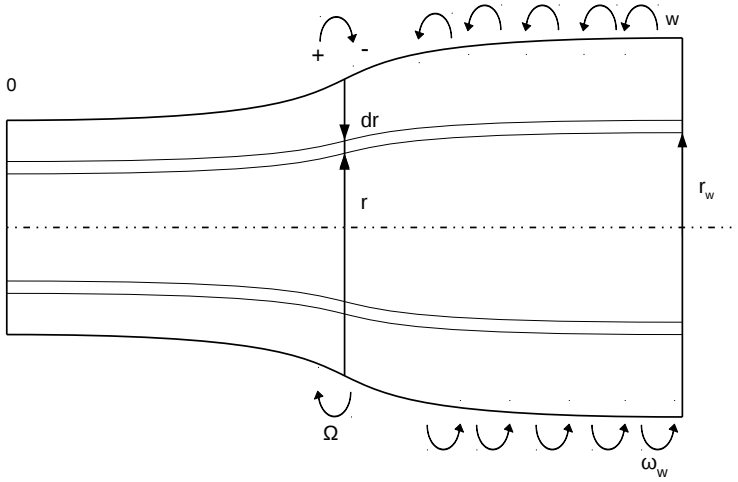

Figure 1. Actuator disc concept

noted U_{rad}. The axial velocity in the far upstream is equal to the free stream U_0. The axial velocity in the rotor ~~plan~~ plane U_n and The axial velocity in the far wake U_{nw} are defined by Eq. (1) and Eq. (2), respectively.

$$U_n(r) = U_0(1 - a(r)) \tag{1}$$

$$U_{nw}(r_w) = U_0(1 - b(r_w)) \tag{2}$$

Where a, a', and b are: the axial induction at the rotor ~~plan~~plane, tangential induction at the rotor plane, and axial induction at the far wake, respectively.

Applying the conservation laws under the assumption of the general momentum theory, the governing equations can be found. The thrust (Eq. (3)) and torque (Eq. (4)) at a given radius of the rotor disc are given by (Sørensen , 2016). The GMT accounts for the pressure drop due to wake rotation, the wake expansion, and the pressure contribution to the lateral force component.

$$C_T = 2b(1-a) + \frac{1-a}{1-b}\frac{p_0 - p_w}{1/2\rho U_0^2} + \frac{1}{1/2\rho U_0^2}\frac{dT_{p,Side}}{dA} \tag{3}$$

$$C_Q = 4a'(1-a)\lambda_r \tag{4}$$

Where, $dT_{p,Side}$ is the pressure contribution to the lateral force component, dA is the elementary disk area, and ρ is the air density. p_w and p_0 are the pressure in the far wake and the atmospheric pressure respectively. $\lambda_r = r\Omega/U_0$ is the speed ratio.

The thrust coefficient in the GMT does not form a closed and solvable system because the unknowns number is too high compared to the number of the equations. Consequently, additional assumptions need to be introduced. ~~The lateral force component, $dT_{p,Side}$ is difficult to determine and can be found using CFD, however, this term is generally considered to be small (Sørensen , 2016). Thus, the annular element are independent of each other. Additionally, modern~~ Modern horizontal axis wind turbines (HAWT) are operating at high rotational speed in order to minimize the wake rotation losses and thus extract more power (Gupta and Leishman , 2005). As a result of high rotational speed, the rotor will have less solidity than a rotor operating at low rotational speed (Burton et al., 2011). Additionally, low solidity wind turbines (typically 7% or less) will result in a low manufacturing cost of the blades (Tangler (2000) and Burton et al. (2011)). As a result, the pressure drop due to wake rotation can also be neglected ($p_0 = p_w$).

The lateral force component, $dT_{p,Side}$ is difficult to determine and can be found using CFD, however, this term is generally considered to be small (Sørensen , 2016). Thus, the annular elements are independent of each other, and the far wake axial induction is taken twice the axial induction at the rotor disc (b=2a), corresponding to Glauert 1D MT model. However, neglecting the lateral force component will result in an unrealistic wake expansion area in the 1D far wake expansion model (Eq. (5)) at higher axial induction (see Fig. 2), which contradict the initial assumption of annular independence. Consequently, Glauert model is only consistent at a very low axial induction factor, where both the governing equation (Eq. (3)) and continuity equation (Eq. (5)) respect the annular independence and small expansion conditions. Glauert model assumes simply that the axial velocity at the rotor disk (U_n) is a mean value of upstream velocity (U_0) and far wake axial velocity (U_{ww}). This relationship is independent of operating conditions and rotor geometry. In order to ensure the small expansion for higher axial induction, the expansion ratio ($\chi = b/a$) needs to be accurately estimated by taking into account the operating conditions and rotor geometry.

$$\frac{r_w}{r} = \sqrt{\frac{1-a}{1-2a}} \tag{5}$$

The thrust coefficient becomes similar to 1D MT except for the expansion effect that is parameterized by the far wake expansion ratio ($\chi = b/a$)~~to be determined~~ . the expansion ratio will be accurately estimated instead of taking $b = 2a$ as the 1D MT. The hypothesis of an infinite number of blades is corrected using the Prandtl tip and hub loss model (Prandtl, 1921) . The thrust and torque are given by Eq. (6) and Eq. (7), respectively.

$$C_T = 2\chi a F(1-a) \tag{6}$$

$$C_Q = 4a' F(1-a)\lambda_r \tag{7}$$

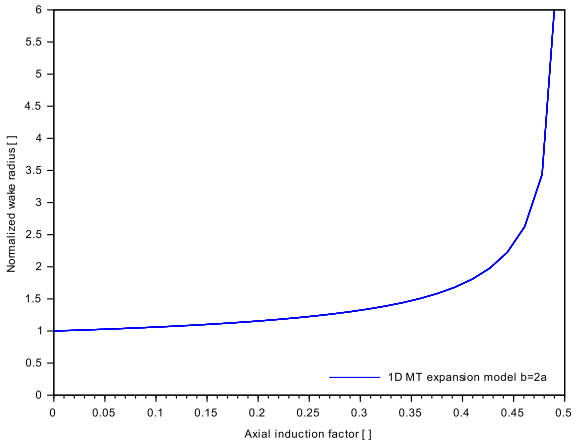

Figure 2. 1D MT Far wake expansion radius as a function of axial induction factor

Prandtl tip and hub loss model $F = F_{tip}F_{hub}$ is given by Eq. (8) and Eq. (9), respectively.

$$F_{tip} = \frac{2}{\pi} cos^{-1}(exp[-\frac{N}{2}\frac{R-r}{rsin(\phi)}]) \tag{8}$$

$$F_{hub} = \frac{2}{\pi} cos^{-1}(exp[-\frac{N}{2}\frac{r-r_h}{r_h sin(\phi)}]) \tag{9}$$

Where ϕ is the inflow angle, R is the tip radius, r_h is the hub radius, and N is the number of blades.

Note that the radial flow is absent in the thrust coefficient equation because of the absence of radial flow in the far upstream and downstream to the actuator disc and it is only present in the near wake, reaching a maximum at the rotor disc when following a streamline (Van Kuik , 2017a). This was proved by Van Kuik (2017a) using vorticity-based arguments. As a result, When applying the conservation of momentum, the radial flow is canceled out, but its effect remains present in the far wake by the far wake expansion ratio.

2.2 New far Wake expansion model

The far wake expansion radius can be found by applying the conservation of the axial flow between the rotor disc and the far wake. It is given by Eq. (10).

$$\frac{r_w}{r} = \sqrt{\frac{1-a}{1-b}} \tag{10}$$

In the case of the 1D MT, the far wake axial induction is taken as twice the axial velocity in the rotor ~~plan~~ plane (b=2a), the 1D far wake expansion radius is given by Eq. (~~??~~5).

$$\frac{r_w}{r} = \sqrt{\frac{1-a}{1-2a}}$$

~~1D MT Far wake expansion radius a a function of axial induction factor~~

One of the major drawbacks of the 1D MT far wake expansion model is the unrealistic expansion when the axial induction is approaching 0.5 as the wake velocity tends to zero as shown in Fig. ~~??~~2. For this reason, the MT is replaced by an empirical equation for axial induction higher than a critical value between 0.2 and 0.4 depending on the empirical model used (Pratumnopharat et al, 2011). Low solidity wind turbines are characterized by small wake expansion compared to high solidity rotors (Sezer-Uzol and Uzol (2013), Sørensen and Kock (1995), and Zahle and Sørensen (2007)).Thus, for a given axial induction factor, the far wake expansion radius for low solidity rotors will be further over-estimated. Consequently, the 1D MT will be valid only for a very low axial induction factor which corresponding to a very low tip speed ratio. This is generally because the far wake expansion ratio in 1D MT is independent of operating conditions and geometry of the wind turbine rotor.

To take into account the operating conditions and rotor ~~'s~~ geometry effects on the far wake expansion ratio. First, the fractional decrease in axial wind speed between the rotor plane and the far wake is defined by Eq. (11). It is a normalized and dimensionless quantity between 0 and 1. In case of no expansion of the wake $\xi = 0$, and the limiting case $\xi = 1$ corresponds to the maximum wake expansion ratio (b=2a) since $b/a < 2$ according to GMT. Second, the classical dimensional analysis (Graebel , 2001) is used to identify all relevant dimensional grouping to the far wake expansion, then applying the Buckingham pi theorem to estimate the fractional decrease in axial wind speed ξ. Hence, the far wake expansion ratio can be computed by ~~$\chi = \xi - 1$~~ $\chi = \xi + 1$.

$$\xi = \frac{b-a}{a} \tag{11}$$

All dimensional parameters that are relevant to the far wake expansion are identified. They are shown in Table 1. The actuator disc geometry parameters include the blade tip radius R, the local radial station r, and the blade number N. The flow conditions are the free stream speed U_0, the rotor rotational speed Ω, and the additional velocity induced by the wake ν (m/s). The classical Buckingham pi theorem states that the number of dimensionless groupings is equal to the number of dimensional parameters subtracted by the number of independent dimensions (length, time). Note that the blade number is already dimensionless. thus, there are a total of three dimensionless groupings: the normalized blade radius, the tip speed ratio, and additional velocity induced by the wake normalized by the free stream. The blade number is the fourth dimensionless number (Table 2).

The above dimensionless grouping can be further reduced to one dimensionless group that characterizes the wake, which is the apparent helical pitch (Eq.12) relating the rotor parameters $(N, \lambda, r/R)$ to the far wake parameters $(\bar{h}, \bar{\nu})$.

$$\bar{h} = \frac{h}{Nr} = \frac{2\pi}{N(r/R)\lambda}(1-\bar{\nu}) \tag{12}$$

Table 1. Parameters relevant to far wake expansion ratio.

Blade geometry	Flow conditions
r R N	U_0 Ω ν

Table 2. Dimensionless groupings relevant to far wake expansion ratio.

Blade geometry	Flow conditions
$\frac{r}{R}$ N	$\lambda = \frac{R\Omega}{U_0}$ $\bar{\nu} = \frac{\nu}{U_0}$

Where, h is the helical pitch of the wake, and $\bar{h}$ is the normalized apparent helical pitch of the wake.

This finding is in accordance with vortex theory, where the far wake parameters (r_w, h, ν) are related to the near wake (r, R, N, λ, C_T) by an expansion model (Okulov et al. (2015)). The thrust coefficient is excluded in this work since it is already depending on the wake expansion and also to avoid a strong coupling of BEM equations. Thus, the dimensionless expansion radius r_w/r depends on the apparent helical pitch$\bar{h}$, dimensionless velocity induced by the wake $\bar{\nu}$. However, according to Okulov et al. (2015), for small expansion of the wake, the additional velocity induced by the wake of the tip vortices equals half the averaged induced axial velocity with a correction of a small expansion ($\epsilon = r_w - r$) as shown in Eq.13. As a result, the velocity induced by the wake has a small variation ($0 \leq \bar{\nu} \leq 0.25(1+\epsilon)$), when the rotor is operating in the momentum region ($0 \leq \ a \leq 0.5$), compared to the apparent helical pitch varying from zero to infinity. Thus, the additional velocity induced by the wake can be neglected and the apparent helical pitch is considered as the most important dimensional parameter.

$$\bar{\nu} = \frac{a}{2}(1 + \frac{\epsilon}{R}) \tag{13}$$

Before applying the Buckingham pi theorem to estimate the fractional decrease in axial wind speed, the normalized apparent helical pitch should be normalized by the relative distance $\sqrt{r^2+h^2}$ instead of the blade radius only. According to the pi theorem, the fractional decrease in axial wind speed is given by Eq. (14). As a result, the far wake expansion ratio is given by Eq. (15).

$$\xi = a_0(\frac{h/N}{r}\frac{r}{\sqrt{(r^2+(h/N)^2}}\frac{r}{\sqrt{r^2+(h/N)^2}})^{b_0} \tag{14}$$

$$\chi(r) = 1 + a_0(\frac{\bar{h}}{\sqrt{1+\bar{h}}}\frac{\bar{h}}{\sqrt{1+\bar{h}^2}})^{b_0} \tag{15}$$

Where a_0 and b_0 are empirical parameters. ~~In this paper, these parameters are taken as~~ First, using the limiting case ($\lambda \to 0$), the parameter a_0 is found to be always equal to unity ($a_0 = 1$). The parameter b_0 has been estimated from experimental data of the NREL phase VI. Only data at one tip speed ratio is enough to estimate b_0. However, in order to cover a broader range of tip speed ratio, we used the data of the NREL phase VI at $U_0 = 5m/s, U_0 = 7m/s$, corresponding to a tip speed of 7.58 and ~~$b_0 = 1$ for the NREL Phase VIrotor~~5.41 respectively. Comparing computed and measured distributions of normal and tangential forces, it was found that $b_0 \approx 1$ gives the best curve fit. Once the far wake expansion ratio is found, the new far wake expansion radius can be computed using Eq.16 as follows:

$$\frac{r_w}{r}(r) = \sqrt{\frac{1 - a(r)}{1 - a(r)\chi(r)}} \tag{16}$$

3 Blade element model accounting for stall delay effect

3.1 Blade element theory

The blade element theory assumes that the blades are made up of a number of blade elements arranged in the spanwise direction, so the airfoil theory can be used to compute the local loads and velocities acting on each blade element. The BET assumes that the blade elements are aerodynamically independent and do not have any interference between them. The loads can be obtained from the 2D lift, drag, and moment coefficients of the airfoil at any radial position. The inflow is known at the blade and a lifting-line assumption is used (Branlard , 2017). As a result of these assumptions, the global loads on a blade can be integrated over the total blade span incorporating the velocity terms, to obtain the thrust, the torque, and power developed by the blade. This is further multiplied by the number of blades to get the total rotor thrust, torque, and power.

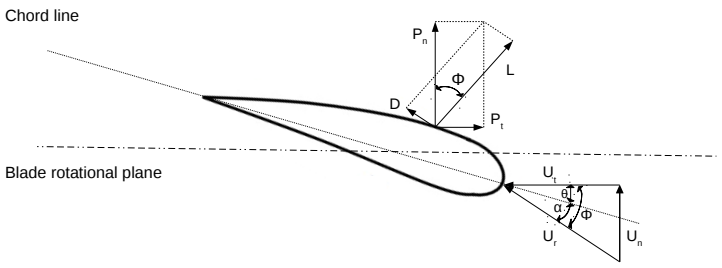

Figure 3. Velocity triangle and resulting aerodynamic ~~foeces~~ forces applied to an airfoil.

A blade element is an infinitesimal fraction dr of the blade radius R at a radial position r, so it can be considered as an airfoil. An airfoil is defined with by its chord c(r), its twist $\theta(r)$ and its shape. The relative wind applied to a blade element, noted $U_{rel}(r)$, is decomposed into a normal component $U_n(r)$ and a tangential component $U_t(r)$ to the rotor plane. Three characteristic angles defined by the velocity axis and the chord axis: the flow angle $\phi(r)$ between the tangential and relative velocity and it is assumed to be known, the airfoil twist $\theta(r)$ about to the rotor plane, and the angle of attack $\alpha(r)$ between the relative velocity and the chord axis and it is related to aerodynamic loads. Since the lifting-line assumption is used, the velocity triangle can be defined in terms of the axial and tangential inductions factors a and a' (Eq. 17 and Eq.18). The relationship between these angles and the velocity components are given in Equations 19 and 20. The blade element, velocity triangle, and aerodynamic forces are shown in Figure 3.

$$U_n = U_0(1-a) \tag{17}$$

$$U_t = \Omega r(1+a') \tag{18}$$

$$tan(\phi) = \frac{U_n}{U_t} \tag{19}$$

$$\alpha = \phi - \theta \tag{20}$$

The lift and drag forces per unit of length applied on the blade element of the surface are defined as follows:

$$L = 1/2\rho c U_{rel}^2 C_{l2D} \tag{21}$$

$$D = 1/2\rho c U_{rel}^2 C_{d2D} \tag{22}$$

Where $(C_{l2D}(\alpha), C_{d2D}(\alpha))$ are the 2D lift and drag coefficients respectively. The normal and tangential forces per unit of length are defined as the projection of the lift and drag on the longitudinal plane and rotor plane (Fig. 3). They can also be defined in the function of normal and tangential coefficients.

$$P_n = 1/2\rho c U_{rel}(C_{l2D}cos(\phi) + C_{d2D}sin(\phi)) = 1/2\rho c U_{rel}^2 C_{n2D} \tag{23}$$

$$P_t = 1/2\rho c U_{rel}^2 (C_{l2D} sin(\phi) - C_{d2D} cos(\phi)) = 1/2\rho c U_{rel}^2 C_{t2D} \quad (24)$$

Since the wind turbine rotor has identical blades, the loading on the blade elements of the blades at the same radius will be also identical. The local thrust, torque and power coefficients applied to an elementary annulus at a radial position r of the rotor disc are defined as follows:

$$C_T = \frac{N P_n dr}{1/2\rho U_0^2 2\pi r dr} = \frac{(1-a)^2}{sin^2(\phi)} \sigma C_{n2D} \quad (25)$$

$$C_Q = \frac{N P_t r dr}{1/2\rho U_0^2 r 2\pi r dr} = \frac{(1-a)(1+a')}{sin(\phi)cos(\phi)} \lambda_r \sigma C_{t2D} \quad (26)$$

$$C_P = C_Q \lambda_r = \frac{(1-a)(1+a')}{sin(\phi)cos(\phi)} \lambda_r^2 \sigma C_{t2D} \quad (27)$$

where $\sigma = Nc/(2\pi r)$ is the local solidity.

3.2 3D stall delay modeling

The stall delay phenomenon is still challenging current 1D models as it was shown by Breton et al. (2008)~~by performing a comparative study of several stall delay model~~. However, Bak et al. (2006) model was found to have superior accuracy thanks to the modeling approach that was based on estimating the pressure gradient due to rotation instead of estimating the loading gradient. Although, Bak model is still over-estimating the loads. In addition, it is not yet ~~fylly~~ fully validated for the spanwise distribution of the loadings. In this work, The stall delay model originally developed by Bak et al. (2006) will be improved based on recent advances in this subject.

3.2.1 Bak model

Bak et al. (2006) was the first to develop a stall delay model that is based on estimating the pressure gradient instead of the force gradient due to the blade rotation. Bak et al. (2006) assumed that the chordwise flow is zero in the separated area, which is the same assumption made by Corten (2001) and (Lindenburg , 2003) to describe the centrifugal pumping mechanism due to rotation. Thus, the radial flow is assumed to be dominant compared to the chordwise flow in separated area. The centrifugal pumping mechanism is described as follows, the centrifugal force induce a radial flow in the separated area, which in turn induce a chordwise Coriolis force that delays separation and amplifies the pressure in separated area. The pressure gradient is defined as the product of two functions: An amplification and a shape. The amplification was estimated as the ratio of the

sum of centrifugal and Coriolis force to the pressure force, these forces were estimated through an order of magnitude analysis of NS equations. The shape was estimated through a simple empirical equation based on fitting the 3D experimental data of NREL phase VI at 30% of the blade radius. The pressure gradient is given by Eq. 28.

$$\Delta C_P = 5(1-\frac{x}{c})(\frac{\alpha-\alpha_0}{\alpha_1-\alpha_0})^2\sqrt{1+(\frac{R}{r})^2}\frac{c}{r}\frac{1}{1+tan^2(\phi)} \tag{28}$$

Where α_0 is the AoA at which the flow begins to separate and α_1 is the AoA at which the flow is completely separated. For the S809 airfoil used in the NREL phase VI rotor. α_1 and α_2 can be approximately taken as 6.2^o and 21^o. x/c is the normalized chord-wise position.

The normal and tangential forces gradient is found by integrating the pressure gradient over the full chord.

$$\Delta C_n = \int_{x/c=0}^{x/c=1} \Delta C_P d(\frac{x}{c}) \tag{29}$$

$$\Delta C_t = \int_{y/c=y/c(leading-edge)}^{y/c=y/c(trailing-edge)} \Delta C_P d(\frac{y}{c}) \tag{30}$$

The 3D normal and tangential force coefficients are computed by

$$C_{n3D}(\alpha) = C_{n2D}(\alpha) + \Delta C_n \tag{31}$$

$$C_{t3D}(\alpha) = C_{t2D}(\alpha) + \Delta C_t \tag{32}$$

3.2.2 Improved Bak model

The stall delay model proposed by Bak ~~assume~~ assumes that the chordwise velocity is zero and the spanwise velocity is dominant when the flow is separated. This hypothesis was also adopted by Corten (2001) based on an experimental study on the flow separation on the wind turbine blade. As a result, this model is only valid inside the separated area where the radial flow is constant. Assuming that the pressure gradient induced by the spanwise flow in the separation area mainly affects the normal force of the local airfoil, since the pressure gradient depends only on the chord-wise position. This is similar to the analysis of (Lindenburg , 2003). The normal force gradient can be computed by integrating the pressure gradient in the

separated area is given by Eq. 33, The proposed improvement is consistent with the centrifugal pumping mechanism and the normal force gradient becomes dependent on the separation factor, which is a measure of the separated area on the airfoil.

$$\Delta C_n = \int_{x/c}^{1} \Delta C_P d(\frac{x}{c}) = \frac{5}{3} f^3 (\frac{\alpha - \alpha_0}{\alpha_1 - \alpha_0})^2 \sqrt{1 + (\frac{R}{r})^2} \frac{c}{r} \frac{1}{1 + tan^2(\phi)} \tag{33}$$

Where $f = 1 - x/c$ is the trailing edge separation factor. It can be estimated using the Kirchhoff-Helmholtz model (Eq. 34) that is commonly used in the dynamic stall computation (Leishman and Beddoes , 1986).

$$f = 1 - \left(2 \sqrt{\frac{C_{n2D}}{(\alpha - \alpha_0)\frac{\partial C_{n2D}}{\partial \alpha}}} - 1\right)^2 \tag{34}$$

Note that the improved bak model is in good agreement with Wang et al. (2013) findings. Since, Wang et al. (2013) solved the inviscid stall delay model developed by Corten (2001). They found that the shape of the normal force gradient to be a third-order ~~plynomial~~ polynomial as a function of the trailing edge separation factor, which is consistent with Eq. 33.

3.2.3 Performance tip loss correction

The blade element theory does not take into account the finite span of the blade; it treats all sections of the blade the same way. In reality, this is not true because there is always aerodynamic loss at the tip of the blade (Shen et al. , 2005). The performance tip loss is used to correct the 3D aerodynamic force coefficients; since the forces should converge to zero at the tip to equalize the pressure between the upper and lower surface of the blade. Shen's tip loss model (Shen et al. , 2005) is used in this paper. It is given by Eq. (35).

$$F_{1tip} = \frac{2}{\pi} cos^{-1}(exp[-h(r)\frac{N}{2}\frac{R-r}{r sin(\phi)}]) \tag{35}$$

$$h_0 = exp[-c_1(N\lambda - c_2)] + 0.1 \tag{36}$$

The correction function h_0 is depending only on the number of blades and the tip speed ratio. The constants c_1 and c_2 are determined from experimental data. In case of the NREL phase VI rotor: $c_1 = 0.125$ and $c_2 = 21$.

The 2D aerodynamic data used in this work are taken from Lindenburg (2003) for the non-rotating blade. The performance tip loss model will be used in both Bak and improved Bak models. The 3D correction of the lift and drag ~~are~~ is given by Eq. (37) and Eq. (38).

$$C_{l3D}(\alpha) = F_{1tip}(C_{l2D}(\alpha) + \Delta C_n cos(\alpha)) \tag{37}$$

$$C_{d3D}(\alpha) = F_{1tip}(C_{d2D}(\alpha) + \Delta C_n sin(\alpha)) \tag{38}$$

4 Improved BEM model

In order to compute the BEM solution (a, a', ϕ), the improved BEM model needs to be completed by ~~respecting the KJ theorem and using a~~ the turbulent wake state model for axial induction factor $a > a_c$. Then, the improved BEM equations will be solved using the guaranteed convergence algorithm to avoid any convergence issues.

4.1 ~~Induced velocities computational method~~

~~The conceptual model of Kutta-Joukowski for the wind turbine rotor is identical to the BET, except for the exclusion of drag force. Since, the induced velocities are produced only by lift force according to vortex theory and particularly the Kutta-Joukowski theorem (Okulov et al. , 2015). As a result, The orthogonality condition must be respected between the total lift force and the relative velocity (see Fig. ??).~~

~~KJ Velocity triangle and resulting aerodynamic foeces applied to an airfoil.~~

~~By applying The Kutta-Joukowski theorem to a blade element of length dr, the total force is given by Eq. (??).~~

$$\boldsymbol{L_{KJ}} = \rho U_{rel} \boldsymbol{\Gamma}$$

~~Where, Γ is the circulation vector defined by Eq. (??).~~

$$\boldsymbol{\Gamma} = 0.5 c U_{rel} \boldsymbol{C_L}$$

~~The local thrust and torque produced at an elementary annulus at a radial position r of the rotor are obtained from the superposition of the local contributions L_{KJ} of each of N blades. The local thrust and torque coefficients applied to an elementary annulus are given by Eq. (??) and Eq. (??).~~

$$CT_{KJ} = \sigma \frac{(1-a)^2}{sin^2(\phi)} C_{l3D} cos(\phi)$$

$$CQ_{KJ} = \frac{(1-a)(1+a')}{sin(\phi)cos(\phi)} \lambda_r \sigma C_{l3D} sin(\phi)$$

The momentum theory is valid up to a critical value of the axial induction factor $(a < a_c)$. For higher induction the wind turbine operating in the turbulent wake state. Thus, an empirical relationship between the thrust coefficient and the axial

induction factor is needed. In this paper, Buhl and Marshall (2005) approach is used because it does not suffer from numerical discontinuity between the theoretical and empirical thrust coefficients, and also it shows a good agreement with experimental data. The proposed correction model is developed following the approach of Buhl and Marshall (2005). The thrust coefficient for the axial induction factor larger than a critical value ($a > a_c = 0.4$) is given by Eq. (39).

$$C_T = \frac{8}{9} + \left(2\chi F - \frac{40}{9}\right)a + \left(\frac{50}{9} - 2\chi F\right)a^2 \tag{39}$$

It is clear that this equation is very similar to the original Buhl and Marshall (2005) correction. Equation 39 can be reduced to that of Buhl if relation the far wake expansion ratio $\chi = 2$.

4.1 ~~Algorithm solution~~

Historically, the solution method for solving the BEM equations is based on taking the axial and tangential induction factors as the unknowns, then solve the fixed-point problem $(a, a') = f(a, a')$ using iterative method. This solution method is simple and fast but suffer from some convergence problems and does not always converge to the right solution (Maniaci , 2011) . Recently Ning (Ning , 2014) proposed a solution method that guaranteed the convergence which is based on reducing the two governing equations of the BEM model to one residual function Eq. (40), then solve it by a root-finding algorithm. The inflow angle is the unknown and not the induction factors used as the unknown in the classical iterative algorithms.

$$f(\phi) = \frac{sin(\phi)}{1-a} - \frac{cos(\phi)}{(1+a')\lambda_r} \tag{40}$$

The momentum/empirical region corresponds to local inflow angles in the range $\phi \in C(]0, \pi[)$. In this case, there is two-equation for the axial induction factor, a criterion is needed to distinct the momentum region ($a < a_c$) and the empirical region ($a > a_c$). The criterion is given by ($\eta_0 = 2/3$). The axial and tangential induction factors can be computed by equating the thrust and torque in the MT and ~~Kutta-Joukowski theory~~BET. The axial and tangential induction factors are given by Eq. (41) and Eq.(42), respectively. The algorithm solution is given below (Algorithm 1).

$$a = \begin{cases} \frac{\eta}{1+\eta} & \eta \leq \eta_0 \\ \frac{\gamma_1 - \sqrt{\gamma_2}}{\gamma_3} & else \end{cases} \tag{41}$$

$$a' = \frac{\eta'}{1-\eta'} \tag{42}$$

Where the parameters η, η', γ_1,γ_1, and γ_3 are depending on the inflow angle. They are defined by:

$$\eta = \sigma C_{n3D}/(2\chi F sin^2(\phi)) \tag{43}$$

$$\eta' = \sigma C_{t3D}/(4Fsin(\phi)cos(\phi)) \tag{44}$$

$$\gamma_1 = \chi F\eta - (10/9 - \chi/2F) \tag{45}$$

$$\gamma_2 = \chi F\eta - \chi/2F(4/3 - \chi/2F) \tag{46}$$

$$\gamma_3 = \chi F\eta - (25/9 - \chi F) \tag{47}$$

~~Once the induced velocities are converged, the performances of the wind turbine rotor can be computed using BET, since the drag force is accounted for when computing the performances of the wind turbine rotor. This is illustrated by the following algorithm.~~

5 Results and discussion

The improved BEM model (N-BEM) will be validated against experimental data of the NREL phase VI rotor, and it is also compared with the classical BEM ~~. However, for briefness and relevance, the~~ model (C-BEM). The validation of the proposed improvements to the BEM method will be done by considering ~~six~~ two different variations of the BEM ~~method~~ model (Table 3)~~, since three modifications to the classical BEM were proposed. First, an evaluation of the effect of the new far wake expansion model and K-J condition on the BEM solution using BEM-KJ-E-0 and BEM-KJ-E-0 models. Second, the validation of the improved stall delay model using BEM-S-0 and BEM-S-1 models. Third, the spanwise distribution of the loading is evaluated and used to identify the wake expansion and stall delay effects on the prediction accuracy using BEM-S-E-0 and BEM-S-E-1 models. Last, An evaluation of the effect of wake expansion and KJ condition on the global loadings using BEM-KJ-E-0 and BEM-KJ-E-0 models~~.

Table 3. BEM model variations.

BEM model variations	Stall delay model	Expansion model
C-BEM	Bak model	1D far wake expansion
N-BEM	Improved Bak model	New far wake expansion

Algorithm 1 Solve ϕ^* for BEM model

function Root(x_l,x_h,f) ▷ Root finding algorithm
  x^* where $f(x^*) = 0$ for $x_l \leq x \leq x_h$ and $f(x_l)f(x_h) < 0$
end function
function $f(\phi)$ ▷ Residual function $f(\phi)$
  if $\eta < \eta_0$ **then**
    $a(\phi) = \frac{\eta}{1+\eta}$
  else
    $a(\phi) = (\gamma_1 - \sqrt{\gamma_2})/\gamma_3$
  end if
  $f(\phi) = \sin(\phi)/(1 - a(\phi)) - \cos(\phi)(1 - \eta'(\phi))/\lambda_r$
end function
function BEM ▷ Main algorithm to solve BEM equations at a given blade radius
  $\epsilon = 10^{-6}$ ▷ Small value to avoid singualrity at $\phi = 0, \pm\pi$
  if $f(\epsilon)f(\pi/2) < 0$ **then** ▷ The solution is within the range $]0, \pi/2[$
    ϕ^*=Root$(\epsilon, \pi/2, f(\phi))$
  else
    if $f(\pi/2)f(\pi - \epsilon) < 0$ **then** ▷ The solution is within the range $]\pi/2, \pi[$
      ϕ^*=Root$(\pi/2, \pi - \epsilon, f(\phi))$
    end if
  end if
  $a = a(\phi)$
  $a' = a'(\phi)$
  $\phi = \text{atan}(\frac{1-a}{\lambda_r(1+a')})$
  $\alpha = \phi - \theta$
  $C_{n3D} = C_{l3D}(\alpha)\cos(\phi) + C_{d3D}(\alpha)\sin(\phi)$
  $C_{t3D} = C_{l3D}(\alpha)\sin(\phi) - C_{d3D}(\alpha)\cos(\phi)$
end function

5.1 3D BEM solution

The spanwise distribution of the converged ~~angles~~ angle of attack for different wind speed is shown in Fig. 4. The ~~BEM-KJ-E,0 and BEM-KJ-E,1~~ C-BEM and N-BEM models are used and compared with the estimated AoA from experimental data given by Sant et al. (2006).

At a low wind speed ($~~U_0 \leq 10~~U_0 < 10$), the drag force is negligible and the wake expansion effect on the AoA is important on the outboard sections of the blade. As a result of the new far wake expansion model (~~BEM-KJ-E,1 model~~N-BEM), the converged angles of attack are in better agreement to experimental data compared ~~using~~ to the 1D far wake expansion model (~~BEM-KJ-E,0model~~C-BEM) that overpredict the AoA. However, at medium to high wind speed ($~~U_0 > 10~~U_0 \geq 10$), the ~~drag force~~ stall delay effect becomes important and the expansion effect is negligible~~(low tip speed) . Additionally, the drag force is further increased~~ . The improved Bak model (N-BEM) gives better agreement to experimental data, and the original Bak model underestimates the AoA at the hub region ~~due to stall delay effect. Consequently, the converged AoA accounting for drag force (BEM-KJ-E,0 model), when solving BEM equations, are over-estimated near the hub region compared to the converged AoA computed by excluding drag force (BEM-KJ-E, 1 model)~~when the flow is not yet fully separated. Once the flow becomes fully separated, both N-BEM and C-BEM models are identical. However, for the full range of operating conditions, some

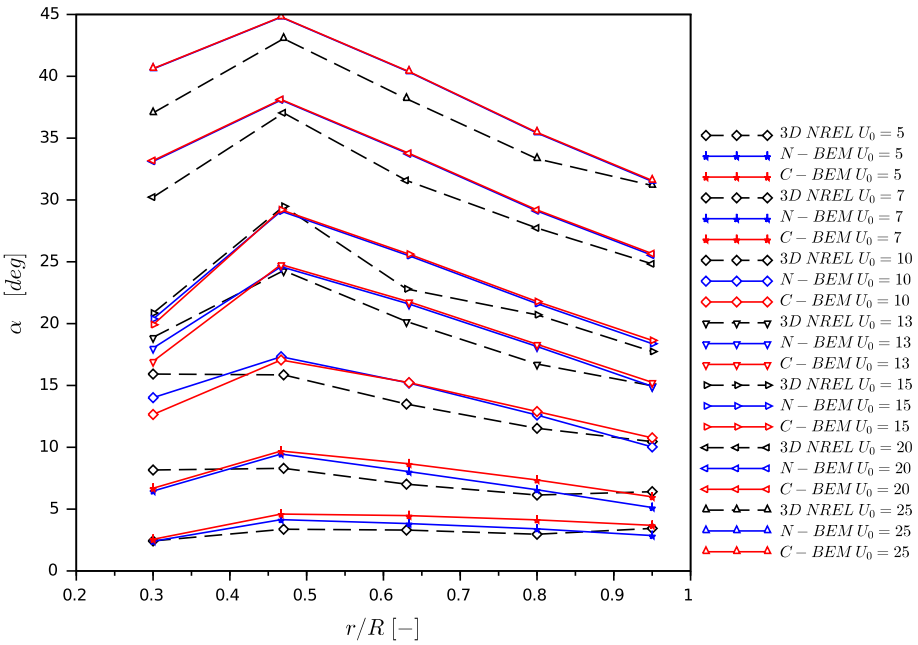

Figure 4. Spanwise distribution of ~~angles~~ angle of attack for different wind speed

inaccuracies of the converged AoA at the tip and hub are mainly due to the tip/hub loss model used. Nevertheless, both models are generally in good agreement with the AoA estimated from 3D NREL phase VI experimental data.

For the NREL phase VI rotor, the axial and tangential induction factors are not available; however, the relative velocity can be estimated from the measured dynamic pressure. The spanwise distribution of the relative velocity, for different wind speed, is shown in Fig. 5. At low wind speed ($~~U_0 \leq 10~~U_0 < 10$), both ~~BEM-KJ-E,0 and BEM-KJ-E,1~~ N-BEM and C-BEM models are accurately predicting the relative velocity of the NREL phase VI rotor ~~, since the drag force is negligible for high tip speed and the~~ since the new far wake expansion model has no noticeable effect on the relative wind speed. As a result, the axial induction factor is under-estimated in ~~BEM-KJ-E,0~~ the C-BEM model since the AoA is over-estimated in ~~BEM-KJ-E,0 modelcompared to BEM-KJ-E, 1 model~~ the C-BEM model. The N-BEM model accurately predicts the axial induction factor at a high tip speed ratio, thanks to the new far wake expansion model (Figure 6). However, at medium to high wind speed (~~$U_0 > 10$), where the drag force becomes important,~~ $U_0 \geq 10$), the relative velocity in ~~the BEM-KJ-E,0 model~~ both C-BEM and N-BEM models diverge progressively toward the hub from the 3D NREL Phase VI experimental data, ~~and the BEM-KJ-E,1 model is accurately predicting the relative velocity for the full blade's span thanks to respecting KJ condition by excluding drag force~~because of the over-estimation of AoA at low tip speed ratio.

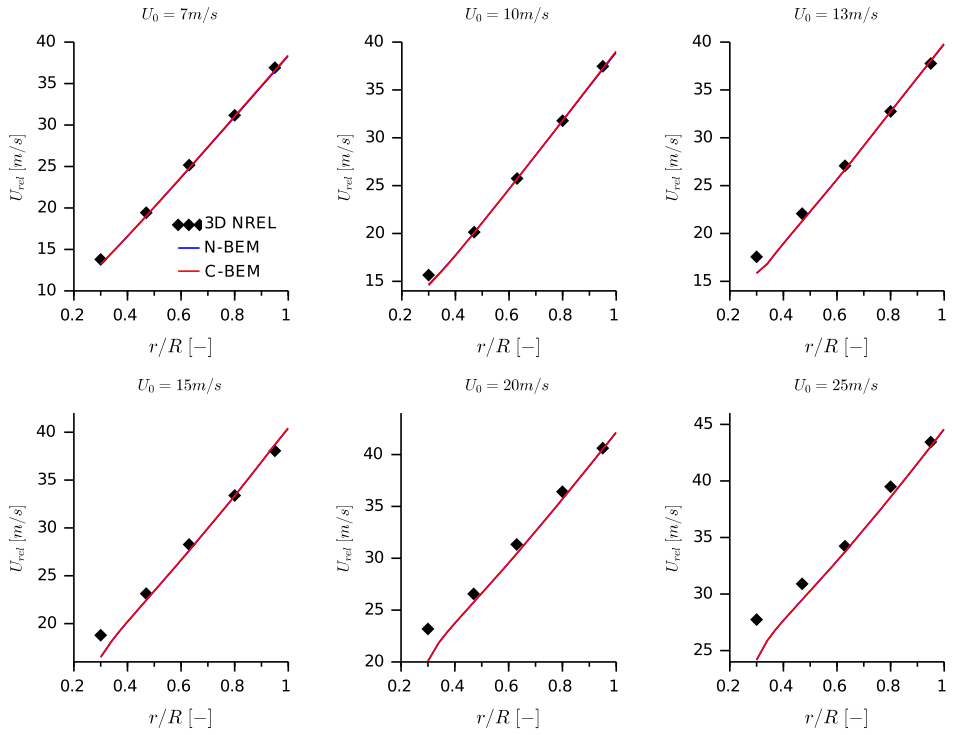

Figure 5. Spanwise distribution of relative velocity for different wind speed

~~Velocity triangle at $r/R = 0.3$ and $U_0 = 20$~~

In order to further highlight the effect of the far wake expansion model on the induced velocities. The relative velocity and inflow angles, at $r/R = 0.8$ and $U_0 = 7$, predicted using the ~~BEM-KJ-E,0 and BEM-KJ-E,1~~ C-BEM and N-BEM models along with the ones estimated from experimental data are given in Figure 6. The axial induction factor ~~predicted using the BEM-KJ-E,0 model~~is ~~under-predicted~~ under-predicted using the C-BEM model, due to the use of the 1D far wake expansion model. However, the new far wake expansion model (N-BEM) improves the prediction of the axial induction factor, and it is in good agreement with the ~~estimate~~ estimated axial induction from experimental data as shown in Fig.6. The tangential induction factor is unchanged for both models since the torque coefficients in both models are identical. The inflow angle predicted using the ~~BEM-KJ-E,1~~ N-BEM model is also improved compared to the ~~BEM-KJ-E,0 model, since~~ C-BEM model. Using the C-BEM, the axial induction is under-estimated and the inflow angle is over-estimated. ~~Thus~~As a result, the new far wake expansion effect is canceled out when computing the relative velocity as shown in Fig.5. This behavior remains valid for other wind speed cases.

~~In order to further highlight the effect of excluding drag force on the induced velocities. The relative velocity and inflow angles, at $r/R = 0.3$ and $U_0 = 20$, predicted using the BEM-KJ-E,0 and BEM-KJ-E,1 models along with the ones from~~

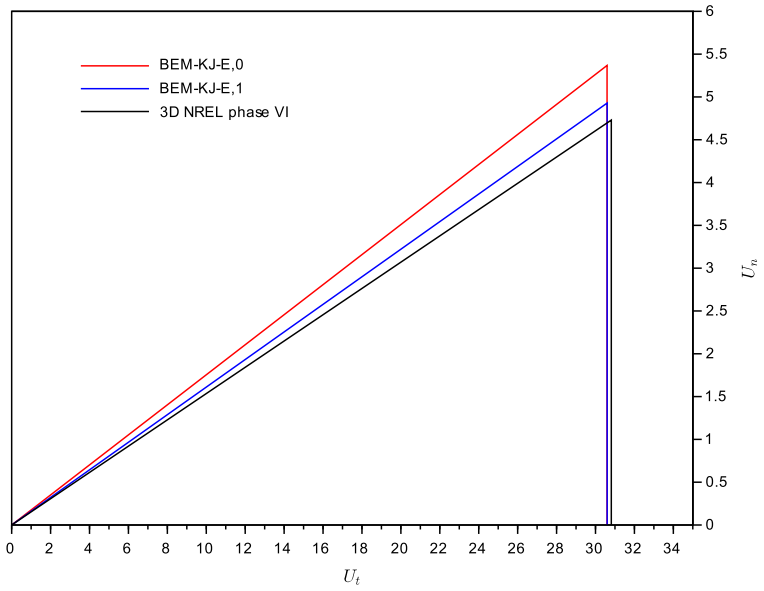

Figure 6. Velocity triangle at $r/R = 0.8$ and $U_0 = 7$

~~experimental data are given in Figure ??. Using the velocity triangle, it is clear that the axial induced velocity is over-estimated in the BEM-KJ-E,0 model, while the tangential induction factor is under-estimated because the drag force is considered when solving the BEM equations, which contradict the KJ theorem. However, When the KJ condition is respected, the axial and tangential induction factors are improved and correlate well with the ones estimated from experimental data. Additionally, the inflow angle is slightly improved as shown in Fig. 4, and the relative velocity is significantly improved as shown in Fig. 5. This behavior remains valid for other wind speed cases.~~

Figure 7 shows the far wake expansion radius, at the free stream $U_0 = 7m/s$, predicted using the ~~BEM-KJ-E,0 and BEM-KJ-E,1~~ N-BEM and C-BEM models. Using the new far wake expansion model, ~~The~~ the improved BEM predict accurately the wake expansion radius compared to the result of Large Eddy Simulation (LES) by Sezer-Uzol and Uzol (2013). However, the 1D MT expansion model ~~used in the BEM-KJ-E,0 model~~ over-estimate the wake expansion radius, especially at high tip speed. It worth mentioning, that for low solidity wind turbines, the wake expansion radius converges a after small distance downstream the rotor plan to an almost cylindrical wake. In the case of the NREL phase VI, the wake radius converges approximatively after one apparent helical pitch (Fig. 7). This was also confirmed by Madsen et al. (2010) showing that the axial velocity converges after just one diameter downstream of the rotor plane. ~~Others like~~ Sørensen and Kock (1995) and Zahle and Sørensen (2007) have also ~~shown~~ found similar behavior.

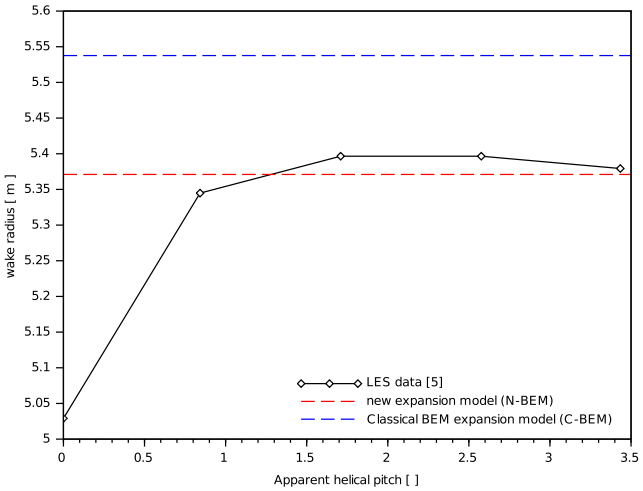

Figure 7. Wake expansion radius at $U_0 = 7$

5.2 3D stall delay model

Figure 8 shows the 3D sectional loading at five radial locations ($r/R = 30\%, 47\%, 63\%, \%80$, and 95%). The ~~BEM-S,0 and BEM-S,1~~ C-BEM and N-BEM models are used to ~~validated~~ validate the improved stall delay model. It can be seen that both stall delay models are identical and predict relatively well the 3D behavior of the rotating blade, except in the separation area ($\alpha_0 < \alpha < \alpha_1$). In the separated area, the improved Bak model predicts accurately the lift and drag coefficients, compared to Bak model that over-predict the lift and drag due to integrating the pressure gradient over the ~~whole~~ full chord. In fact, both stall delay models are only valid in the separated area where the radial flow is dominant compared to the chordwise flow. As a result, the pressure gradient is strongly dependent on the AoA, especially in the separation area, which was recently confirmed by Mauro et al. (2018) using CFD simulation. At $r/R = 95\%$~~)~~, the predicted loadings are in good agreement with experimental data, thanks to Shen tip loss model that is used to correct the lift and ~~frag~~ drag coefficients in both stall delay models.

In both stall delay models, the amplitude of the pressure gradient depends on external forces at a given spanwise position, and the shape of the pressure gradient depends on the AoA and it is strongly empirical. Since it is taken from the 2D airfoil, then corrected using an empirical quadratic function. The amplitude is generally in good agreement with experimental data (Fig.~~10~~ 9 and Fig.~~11~~10), however, some over-estimation and under-estimation of sectional loadings are due to the shape of the pressure gradient that is strongly empirical and needs to be further studied. In fact, the shape of the pressure gradient can vary from triangular shape to trapezoidal shape depending on the separation type: leading-edge separation or trailing edge separation. Schreck and Robinson (2002) has analyzed the pressure data on the NREL Unsteady Aerodynamics Experiment and found out that the 3D pressure coefficients have a trapezoidal as well as triangular shapes. The pressure shape variation was

attributed to various mechanisms mediated by Coriolis and centrifugal forces and also to the presence of an energetic vortex structure.

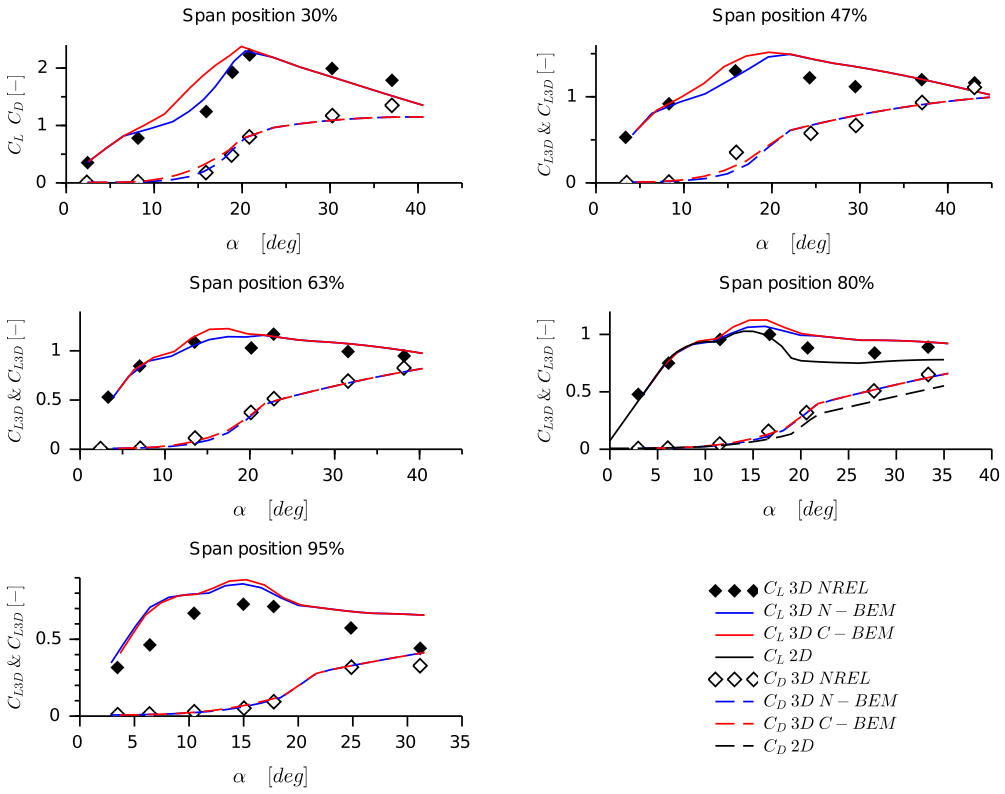

Figure 8. 3D sectional lift and drag coefficients

5.3 Local aerodynamic loadings

Figure 9 and 10 shows the normal and tangential force coefficient along the blade span for six different wind speed. The ~~BEM-S-E,0 and BEM-S-E,1 model~~ C-BEM and N-BEM models are used to evaluate the effect of far wake expansion and stall delay on the spanwise distribution of normal and tangential forces coefficients. The ~~BEM-S-E,1 model agree~~ N-BEM model agrees very well with experimental data for the full range of operating conditions, compared to the ~~BEM-S-E,0~~ C-BEM model that over-predict the loading due to both using the 1D MT expansion model and the stall delay model of Bak. ~~At hight tip speed ($U_0 \leq 10m/s$), the~~ The over-estimation of ~~loadings by the BEM-S-E, 0 is~~ spanwise loading, at $U_0 = 5$, is entirely due to the use of the 1D ~~MT expansion model, that results in an over-estimation of the AoA, resulting in an~~ expansion model. A special case at $U_0 = 7m/s$ where the over-estimation of ~~normal force coefficient. At low tip speed ($U_0 \geq 10m/s$)~~loading is due to both stall delay model at inboard sections and wake expansion at the outboard sections. At $U_0 = 10m/s$, the stall delay

of Bak is responsible for the over-estimation of the spanwise distribution of both normal and tangential force coefficients~~at the hub region and at $U_0 = 7, 10m/s$, which is corresponding to the separation area~~. For the fully separated flow, both stall delay models are identical and they are in good agreement with experimental data. ~~A special case at $U_0 = 7m/s$ where the over-estimation of loading is due to both stall delay model at inboard sections and wake expansion at the outboard sections.~~

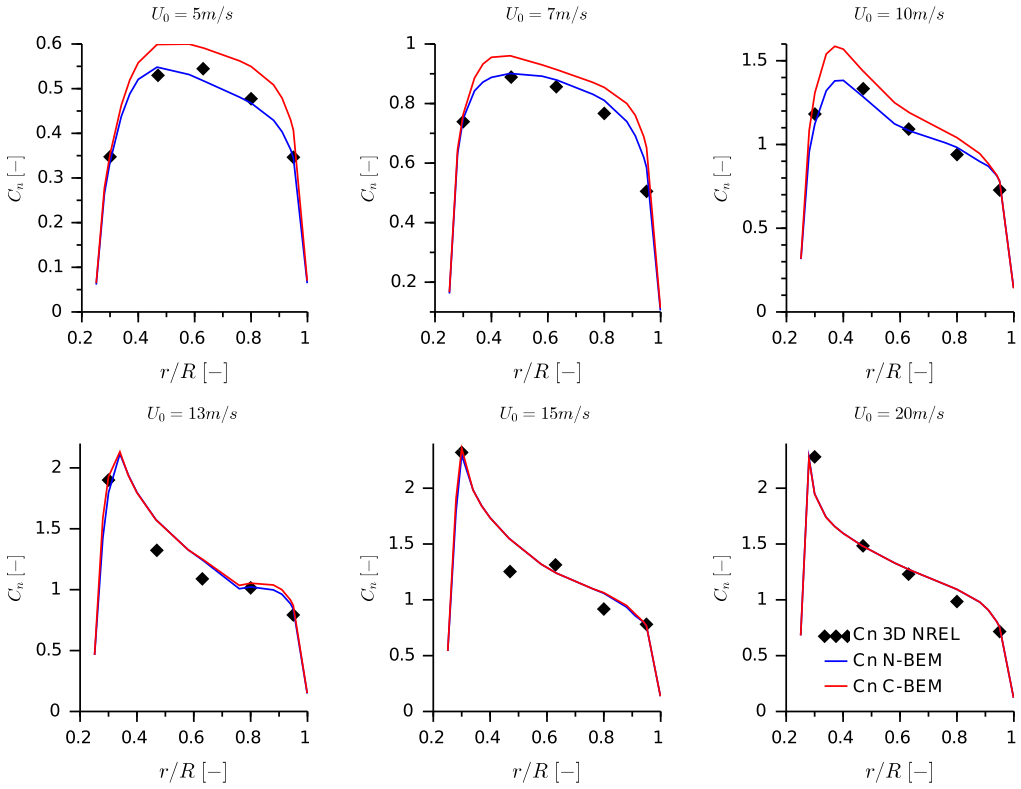

Figure 9. Spanwise distribution of the 3D normal force coefficient for different wind speed

5.4 Global aerodynamic loadings

~~In order to see the far wake expansion and the KJ condition effect on the global performances, the classical BEM and the improved BEM are coupled with the improved stall delay model.~~

The power and thrust forces of the NREL Phase VI rotor for both ~~BEM-KJ-E,0 and BEM-KJ-E,0~~ C-BEM and N-BEM models are shown in Fig. 11. It can be seen that both models are predicting relatively well the power and thrust forces for the full range of operating conditions. However, at low wind speed (high tip speed) the power and thrust forces predicted using the ~~BEM-KJ-E,0~~ C-BEM model, are slightly overestimated compared to the ~~BEM-KJ-E,0 model that account~~ N-BEM model that accounts accurately for the far wake expansion effect. At medium to high wind speed (low tip speed), the power and thrust

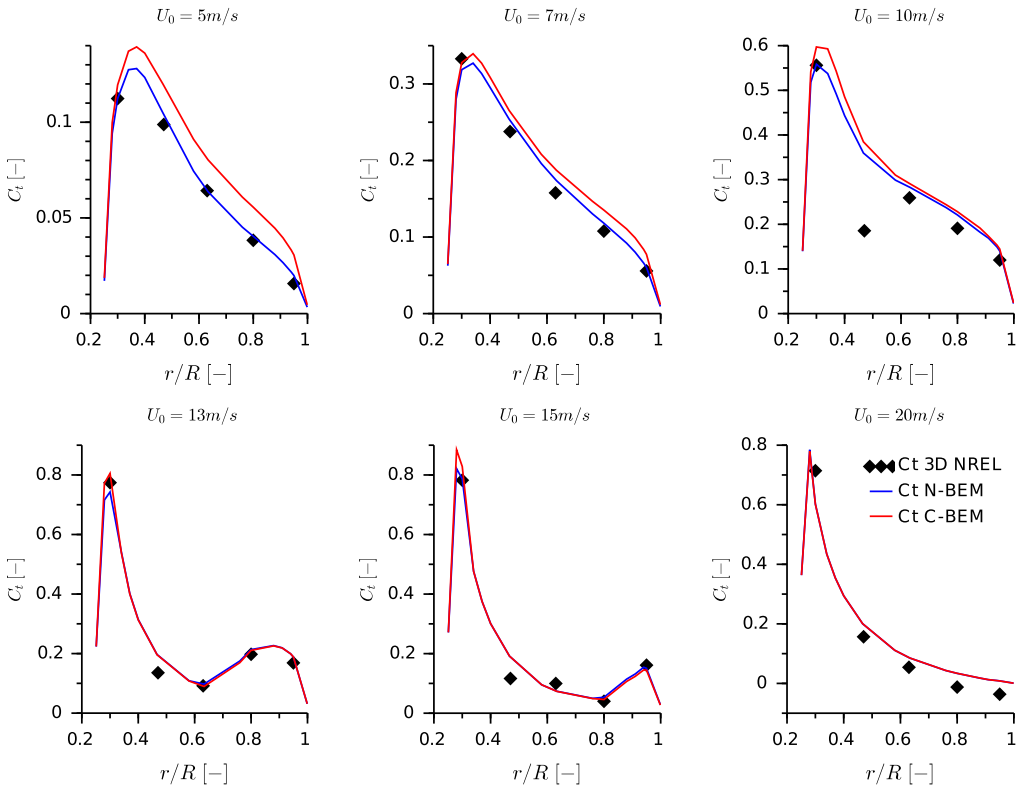

Figure 10. Spanwise distribution of the 3D tangential force coefficient for different wind speed

curves predicted using ~~the BEM-KJ-E,0 model are~~ both models are slightly under-predicted compared ~~to the BEM-KJ-E, 0 model that predicts accurately the power and thrust force, thanks to respecting the Kutta-Joukowski condition~~experimental data, because the relative velocity is under-estimated at the hub region (Figure 5).

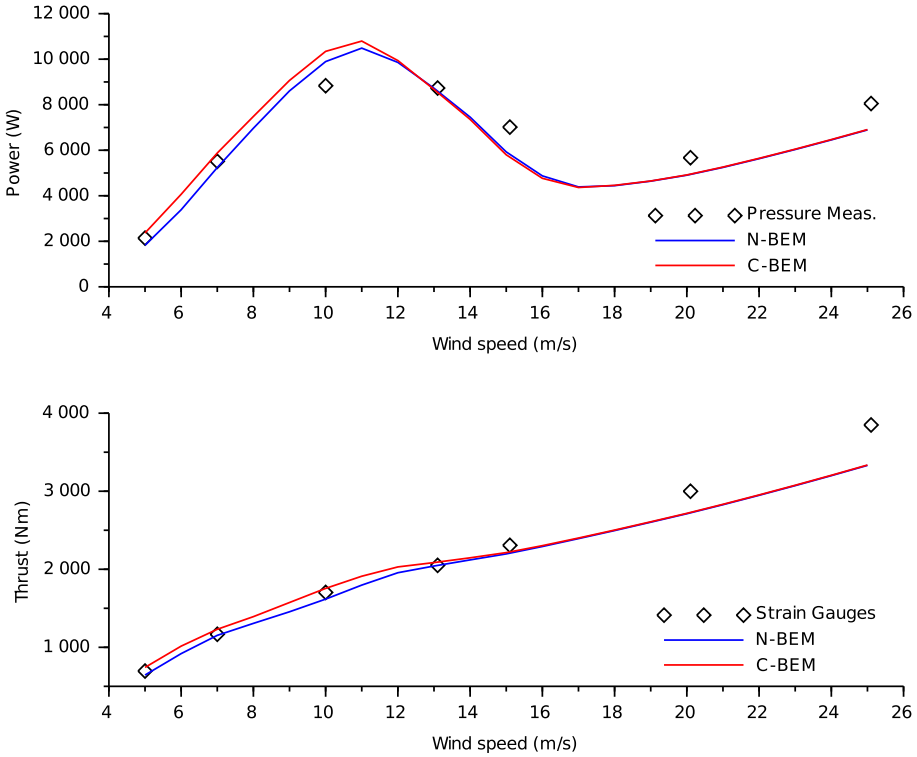

Figure 11. Trust and power for different wind speed

6 Conclusions

In this paper, ~~a state of the art~~ an improved BEM model is developed for aerodynamic prediction of horizontal axis wind turbine rotor. The GMT is applied to low solidity rotors, then a new far wake expansion model is proposed using dimensional analysis. Three-dimensional effects on a rotating blade were estimated using an improved stall delay model based on Bak model. ~~An improved solution method was given for the improved BEM model by respecting Kutta-Joukowski theorem and using the guaranteed convergence algorithm to solve the BEM equations.~~ The improved BEM model is then compared against the classical BEM and the experimental data from the NREL phase VI rotor. The results show a remarkable agreement with experimental data. Additionally, the proposed improvements to the classical BEM requires virtually no additional computational time.

The new far wake expansion model was found to improve the spanwise loading and global loadings at a high tip speed ratio, compared to the 1D MT expansion model that over-predict both the spanwise loading and global loadings. As for the induced velocities, it was found that the axial induction factor was under-predicted using the 1D MT expansion model. While

using the new far wake expansion model results in an accurate estimation of the axial induction factor. Additionally, The 1D MT expansion model over-predict the far wake expansion radius, while the new far wake expansion model predicts accurately the wake expansion radius. However, The new far wake expansion model can be further improved by taking into account the additional velocity induced by the wake.

~~It was also found that accounting for drag force when solving BEM equations results in an important under-prediction of the relative velocity in the hub region, while the converged AoA remains approximately unchanged. As for the induced velocities, it was found that the axial induced velocity is over-estimation while the tangential induction factor is under-estimation in the hub region. The thrust and torque forces were also under-predicted if the drag force is accounted for in BEM equations. In contrast, excluding the drag force when computing the induced velocities, will result in an accurate prediction of the BEM solution (axial induction, tangential induction, and inflow angle). Thus, local and global loadings were accurately predicted.~~

The three-dimensional effects on a rotating blade were accurately estimated using the improved stall delay model compared to the original Bak model. However, Both models are still strongly empirical, especially the shape of the pressure gradient. As a result, the chordwise pressure on a rotating blade needed to be further carefully analyzed in order to improve our understanding of this complex phenomenon, thus accurately modeling the shape of the pressure gradient.

Author contributions. The developpement, implementation, and analysis of the improved BEM model was performed by YO, under the supervision of AA. The preparation of the paper was performed by YO. AA provided assistance with the proof reading of the manuscript.

Competing interests. The authors declare that they have no conflict of interest

Acknowledgements. This work was supported by the NATO Science for peace grant program (SfP-982620) and the Moulay Ismail University within the framework of its research support program 2018.

References

Bak, C., Johansen, J., & Andersen, P. B.: Three-dimensional corrections of airfoil characteristics based on pressure distributions. In Proceedings of the European Wind Energy Conference 1-10, 2006.

Branlard E.: Wind turbine aerodynamics and vorticity-based methods. Vol. 10. New York: Springer, 2017.

Breton SP, Coton FN, Moe G.: A study on rotational effects and different stall delay models using a prescribed wake vortex scheme and NREL phase VI experiment data. Wind Energy: An International Journal for Progress and Applications in Wind Power Conversion Technology. 11(5), 459-82, 2008.

Buhl Jr, Marshall L.: New empirical relationship between thrust coefficient and induction factor for the turbulent windmill state. No. NREL/TP-500-36834. National Renewable Energy Lab.(NREL), Golden, CO (United States), 2005.

Burton T.: Wind Energy Handbook, John Wiley & Sons, 2001

Burton T., Jenkins N., Sharpe D. and Bossanyi, E.: Wind energy handbook, John Wiley & Sons, 2011

Butterfield, C.P., Scott, G. and Musial, W.: Comparison of wind tunnel airfoil performance data with wind turbine blade data. Journal of solar energy engineering 114.2 119-124, 1992.

Carrión M, Steijl R, Woodgate M, Barakos G, Munduate X, Gomez-Iradi S.: Computational fluid dynamics analysis of the wake behind the MEXICO rotor in axial flow conditions. Wind Energy 18.6 1023-1045, 2015.

Clifton-Smith, M. J. : Wind turbine blade optimisation with tip loss corrections. Wind Engineering, 33(5), 477-496, 2009.

Corten, GP.: Inviscid stall model. Netherlands Energy Research Foundation, 2001.

De Vries O.: Fluid dynamic aspects of wind energy conversion. AGARD Advisory Group for Aerospace Research & Development AGARD-AG-243. C4–C9, 1979.

Døssing M, Madsen HA, Bak C.: Aerodynamic optimization of wind turbine rotors using a blade element momentum method with corrections for wake rotation and expansion. Wind Energy 15.4, 2012.

Froude W.: On the mechanical principles of the action of propellers, Trans. Inst. Nav. Archit, 1878.

Glauert, H.: Airplane propellers. In: Durand, W.F. (ed.) Aerodynamic theory (Division L) vol. IV IV, 169-360. Springer, Berlin, 1935.

Goorjian, PM.: An invalid equation in the general momentum theory of actuator disk, AIAA Journal 10.4 543-544, 1972.

Graebel, W.: Engineering Fluid Mechanics. Taylor Francis, 2001.

Gupta S, Leishman J.: Comparison of momentum and vortex methods for the aerodynamic analysis of wind turbines. 43rd AIAA Aerospace Sciences Meeting and Exhibit, 2005.

Hand MM, Simms DA, Fingersh LJ, Jager DW, Cotrell JR, Schreck S, Larwood SM.: Unsteady aerodynamics experiment phase VI: wind tunnel test configurations and available data campaigns. No.NREL/TP-500-29955, National Renewable Energy Lab., Golden, CO.(US), 2001.

Hansen M.O.: Aerodynamics of wind turbines, Routledge, 2015

Herráez I, Stoevesandt B, Peinke J.: Insight into rotational effects on a wind turbine blade using Navier–Stokes computations, Energies 7.10 6798-6822, 2014.

Johansen J, Sørensen NN.: Aerofoil characteristics from 3D CFD rotor computations. Wind Energy: An International Journal for Progress and Applications in Wind Power Conversion Technology 7.4 283-294, 2004.

Joukowski, N.E.: Vortex theory of a rowing screw., Tr. Otd. Fiz. Nauk.Obshchestva Lubitelei Estestvozn, 16 (1), 1912.

Lee HM, Wu Y.: An experimental study of stall delay on the blade of a horizontal-axis wind turbine using tomographic particle image velocimetry. Journal of Wind Engineering and Industrial Aerodynamics Elsevier, 123: 56-68, 2013.

Leishman J. G. and Beddoes T. S.: A generalised model for airfoil unsteady aerodynamic behaviour and dynamic stall using the indicial method, in 42th Annual Forum of the American Helicopter Society 243–265, Washington, 1986.

Limacher, E. J., Wood, D. H.: Derivation of an Impulse Equation for Wind Turbine Thrust. Wind Energy Science, 2020.

Lindenburg C.: Investigation into rotor blade aerodynamics, Energy research Centre of the Netherlands, Report ECN-C–0–025, 2003.

Lock, C.N.H., Bateman, H., Townend, H.C.H.: An extension of the vortex theory of airscrews with applications to airscrews of small pitch, including experimental results. ARC R & M, No. 1014, 1925.

Mauro S, Lanzafame R, Messina M, Brusca S.: A Detailed Analysis of the Centrifugal Pumping Phenomenon in HAWTs Through the Use of CFD Models. Colloquium on Research and Innovation on Wind Energy on Exploitation in Urban Environment Colloquium. Springer, Cham, 2018.

Madsen HA, Bak C, Døssing M, Mikkelsen R, Øye S.: Validation and modification of the blade element momentum theory based on comparisons with actuator disc simulations. Wind Energy: An International Journal for Progress and Applications in Wind Power Conversion Technology 13.4, 373-389, 2010.

Maniaci D.: An investigation of WT-perf convergence issues. 49th AIAA Aerospace Sciences Meeting including the New Horizons Forum and Aerospace Exposition. 2011.

Mast EH, Vermeer LJ, Van Bussel GJ.: Estimation of the circulation distribution on a rotor blade from detailed near wake velocities. Wind Energy: An International Journal for Progress and Applications in Wind Power Conversion Technology 7.3, 189-209, 2004.

McCutchen, C. W.: A theorem on swirl loss in propeller wakes. Journal of Aircraft, 22(4), 344-346, 1985.

Micallef D, van Bussel G, Ferreira CS, Sant T.: An investigation of radial velocities for a horizontal axis wind turbine in axial and yawed flows. Wind Energy 16.4, 529-544, 2013.

Ning, SA.: A simple solution method for the blade element momentum equations with guaranteed convergence. Wind Energy 17.9, 1327-1345, 2014.

Okulov VL, Sørensen JN, Wood DH.: The rotor theories by Professor Joukowsky: Vortex theories. Progress in aerospace sciences 73, 19-46, 2015.

Prandtl, L.: Applications of modern hydrodynamics to aeronautics, (Tech- nical report No. 116). National Advisory Committee for Aeronautics (NACA), 1921.

Pratumnopharat P, Leung PS.: Validation of various windmill brake state models used by blade element momentum calculation. Renewable energy 36.11, 3222-3227, 2011.

Rankine, W. J. M.: On the Mechanical Principles of the Action of Propellers. Transactions, Institute of Naval Architects, Vol. 6: pp. 13-30.

Sant T, van Kuik G, Van Bussel GJ.: Estimating the angle of attack from blade pressure measurements on the NREL phase VI rotor using a free wake vortex model: axial conditions. Wind Energy: An International Journal for Progress and Applications in Wind Power Conversion Technology 9.6, 549-577, 2006.

Schreck S, Robinson M.: Rotational augmentation of horizontal axis wind turbine blade aerodynamic response. Wind Energy: An International Journal for Progress and Applications in Wind Power Conversion Technology 5.2-3, 133-150 2002.

Sezer-Uzol N, Uzol O.: Effect of steady and transient wind shear on the wake structure and performance of a horizontal axis wind turbine rotor. Wind Energy 16.1, 1-17, 2013.

Sharpe D.J.: A general momentum theory applied to an energy-extracting actuator disc, Wind Energy 7 (3), 2004.

Shen WZ, Mikkelsen R, Sørensen JN, Bak C.: Tip loss corrections for wind turbine computations. Wind Energy: An International Journal for Progress and Applications in Wind Power Conversion Technology 8.4, 457-475, 2005.

Schmitz, S., Maniaci, D. C. : Methodology to determine a tip-loss factor for highly loaded wind turbines. AIAA Journal, 55(2), 341-351. 2017.

Snel H, Houwink R, Bosschers J.: Sectional prediction of lift coefficients on rotating wind turbine blades in stall. ECN-C-93-052, ECN, Petten, 1993.

Sørensen JN, Kock CW.: A model for unsteady rotor aerodynamics. Journal of wind engineering and industrial aerodynamics 58.3, 259-275, 1995.

Sørensen JN, Shen WZ, Munduate X.: Analysis of wake states by a full-field actuator disc model. Wind Energy: An International Journal for Progress and Applications in Wind Power Conversion Technology 1.2, 73-88, 1998.

Sørensen, JN.: General momentum theory for horizontal axis wind turbines. Vol. 4. Switzerland: Springer, 2016.

Sørensen, Jens N., and Gijs AM van Kuik. : General momentum theory for wind turbines at low tip speed ratios. Wind Energy 14.7 (2011): 821-839.

Spera DA., Wilson RE.: Wind turbine technology : fundamental concepts of wind turbine engineering. Second Edition, 2009

Sun Z, Chen J, Shen WZ, Zhu WJ.: Improved blade element momentum theory for wind turbine aerodynamic computations. Renewable energy 96, 824-831, 2016.

Tangler James L. : The Evolution of Rotor and Blade Design, 2000

TanglerJ.: The nebulous art of using wind-tunnel airfoil data for predicting rotor performance, ASME 2002 Wind Energy Symposium. American Society of Mechanical Engineers, 2002.

Van Kuik GA.: Joukowsky actuator disc momentum theory. Wind Energy Science 2.1, 307, 2017.

Van Kuik GA, Lignarolo LE.: Potential flow solutions for energy extracting actuator disc flows. Wind Energy 19.8, 1391-1406, 2016.

Vaz JR, Pinho JT, Mesquita AL.: An extension of BEM method applied to horizontal-axis wind turbine design. Renewable Energy 36.6, 1734-1740, 2011.

Wang Q, Xu Y, Song JJ, Li CF, Ren PF, Xu JZ.: 3D stall delay effect modeling and aerodynamic analysis of swept-blade wind turbine. Journal of Renewable and Sustainable Energy 5.6, 2013.

Whale J, Anderson CG, Bareiss R, Wagner S.: An experimental and numerical study of the vortex structure in the wake of a wind turbine. Journal of Wind Engineering and Industrial Aerodynamics 84.1, 1-21, 2000.

Wilson RE, Lissaman PBS.: Applied aerodynamics of wind power machines, Oregon State University, May 1974.

Wimshurst, A., Willden, R. H. J. : Computational observations of the tip loss mechanism experienced by horizontal axis rotors. Wind Energy, 21(7), 544-557, 2018.

Wimshurst, A., & Willden, R. H. J. : Analysis of a tip correction factor for horizontal axis turbines. Wind Energy, 20(9), 1515-1528, 2017.

Wood, D. H., Okulov, V. L., Bhattacharjee, D. : Direct calculation of wind turbine tip loss. Renewable Energy, 95, 269-276, 2016.

Wood, D. H., Okulov, V. L. :Nonlinear blade element-momentum analysis of Betz-Goldstein rotors. Renewable Energy, 107, 542-549, 2017.

Wood, D. H.: Including swirl in the actuator disk analysis of wind turbines. Wind Engineering, 31(5), 317-323, 2007.

Xiros MI, Xiros NI.: Remarks on wind turbine power absorption increase by including the axial force due to the radial pressure gradient in the general momentum theory. Wind Energy10: 99–102, 2007.

Zahle F, Sørensen NN.: On the influence of far-wake resolution on wind turbine flow simulations. Journal of Physics: Conference Series. Vol. 75. No. 1. IOP Publishing, 2007.